

Alkyl Chain Length Effects of Polymer Donors on the Morphology and Device Performance of Polymer Solar Cells with Different Acceptors

Shuting Pang, Ruiwen Zhang, Chunhui Duan,* Song Zhang, Xiaodan Gu,* Xi Liu, Fei Huang,* and Yong Cao

Dedicated to Prof. René A. J. Janssen on the occasion of his 60th birthday

The development of nonfullerene acceptors has brought polymer solar cells into a new era. Maximizing the performance of nonfullerene solar cells needs appropriate polymer donors that match with the acceptors in both electrical and morphological properties. So far, the design rationales for polymer donors are mainly borrowed from fullerene-based solar cells, which are not necessarily applicable to nonfullerene solar cells. In this work, the influence of side chain length of polymer donors based on a set of random terpolymers PTAZ-TPD10-*C_n* on the device performance of polymer solar cells is investigated with three different acceptor materials, i.e., a fullerene acceptor [70]PCBM, a polymer acceptor N2200, and a fused-ring molecular acceptor ITIC. Shortening the side chains of polymer donors improves the device performance of [70]PCBM-based devices, but deteriorates the N2200- and ITIC-based devices. Morphology studies unveil that the miscibility between donor and acceptor in blend films depends on the side chain length of polymer donors. Upon shortening the side chains of the polymer donors, the miscibility between the donor and acceptor increases for the [70]PCBM-based blends, but decreases for the N2200- and ITIC-based blends. These findings provide new guidelines for the development of polymer donors to match with emerging nonfullerene acceptors.

1. Introduction

In the past two decades polymer solar cells (PSCs) based on bulk heterojunction (BHJ) concept have attracted considerable attention due to their promising potential as a practical


renewable energy technology.^[1] Significant progresses have been achieved with the witness of power conversion efficiencies (PCEs) increased from 5% to 17% in the past ten years.^[2] Moreover, it is reported that the device lifetime approaching ten years is reachable for PSCs.^[3] These improvements mainly benefitted from the development of nonfullerene acceptors, which can overcome the drawbacks associated with fullerene acceptors and thereby bring PSCs into a new era.^[4] As one of the two core components in a BHJ blend, polymer donors play a critical role in producing high performance PSCs. Therefore, understanding the influence of the chemical structure of polymer donors on the device performance is important to the development of new materials for more efficient PSCs.^[5] Historically, the understandings of the relationship between the chemical structure of photovoltaic polymers and device performance have contributed significantly to the progress of fullerene-based PSCs.^[5] For example,

it is now well recognized that improving the coplanarity of the polymer backbone and polymer crystallinity are favorable for device performance via facilitating the formation of pure polymer domains in blend films, improving charge transport, and suppressing charge carrier recombination.^[6] It is also well known that the molecular weight of polymers is an important factor that influences the device performance of PSCs.^[7] Generally, the device performance of PSCs improves when increasing the molecular weight of polymer donors within polymer solubility limits.^[7]

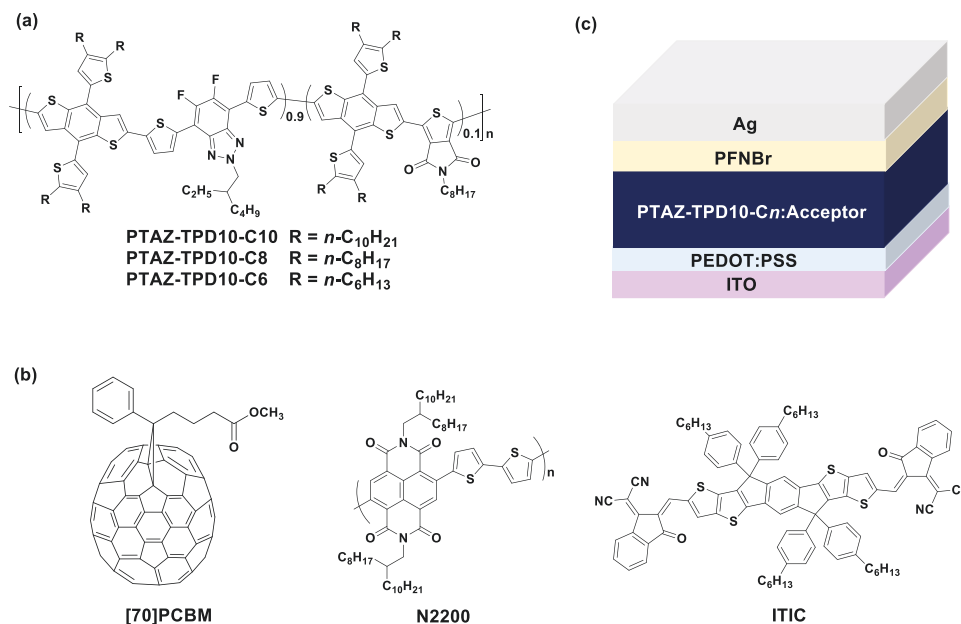
However, the polymer design rationales established for fullerene-based PSCs are not necessarily applicable to nonfullerene PSCs. For example, strong aggregation and high crystallinity of polymer donors are desired for high performance fullerene-based PSCs, but these features are harmful to nonfullerene PSCs.^[8] On the other hand, Marks' group demonstrated that the maximum PCE of all-polymer solar cells is achieved at medium polymer molecular weights rather than high molecular weights.^[9] These findings are contradictory to

S. Pang, R. Zhang, Prof. C. Duan, X. Liu, Prof. F. Huang, Prof. Y. Cao
Institute of Polymer Optoelectronic Materials and Devices
State Key Laboratory of Luminescent Materials and Devices
South China University of Technology
Guangzhou 510640, P. R. China
E-mail: duanchunhui@scut.edu.cn; msfhuang@scut.edu.cn

S. Zhang, Prof. X. Gu
School of Polymer Science and Engineering
University of Southern Mississippi
Hattiesburg, MS 39406, USA
E-mail: Xiaodan.gu@usm.edu

 The ORCID identification number(s) for the author(s) of this article can be found under <https://doi.org/10.1002/aenm.201901740>.

DOI: 10.1002/aenm.201901740



Scheme 1. a) Chemical structures of the PTAZ-TPD10-C_n polymers, b) chemical structures of the electron acceptors [70]PCBM, N2200, and ITIC, and c) device structure employed in this study.

the knowledge obtained from fullerene-based solar cells. In fact, many state-of-the-art polymer donors for fullerene-based PSCs are not successful when combined with nonfullerene acceptors. So far, the electron donors for high efficiency nonfullerene PSCs are mainly limited to the polymers based on benzo-[1,2-*c*:4,5-*c'*]dithiophene-4,8-dione and benzo[*d*][1,2,3] triazole.^[10] Moreover, the development of polymer donors for efficient nonfullerene PSCs usually adopts a trial-and-error procedure due to the lack of unambiguous structure–property relationships to guide the polymer design.^[11] Therefore, any insightful understanding of the influence of the chemical structures on the device performance is very important to the development of polymer donors for nonfullerene PSCs.

Among various structural factors, the alkyl side chain is a critical one that determines the properties of conjugated polymers because it not only serves as solubilizing group but also affects the morphology of resulting blend films greatly.^[12] For example, it was reported that the side chain of polymer donors dominates the formation of fibrillar microstructure and phase separation of BHJ blends.^[12a,b] Too long side chains cause serious liquid–liquid phase separation during film deposition, resulting in excessively large domain sizes in blend films.^[13] Chen et al. demonstrated that the side chain regiochemistry has a significant influence on the intrinsic aggregation properties of polymer donors, the domain size of blend films, and the performance of the resulting nonfullerene PSCs.^[14] Very recently, Tajima's group revealed that the substitution pattern of linear and branched alkyl side chains on polymer donors can control the positions of fullerene acceptor molecule around the π -conjugated main chains of polymer donors in BHJ blends.^[15] The side chain pattern that allows an electron-accepting unit of polymer main chain positioned in close proximity to fullerene produced higher performance in PSC devices. In short, these studies demonstrated the importance of alkyl side chain for the performance of polymer donors. Therefore, it is of profound

importance to understand the side chain effect of donor polymers on the device performance of PSCs, particularly when the polymers are combined with different electron acceptors.

In this work, we investigate this by synthesizing a set of random terpolymers PTAZ-TPD10-C_n consisting of alkylthienylbenzodithiophene (BDT), difluorinatedbenzotriazole (TAZ), and thienopyrroledione (TPD) as the polymer donors. The conjugated backbones of the polymers are identical but the side chains on BDT units differ in length. As shown in **Scheme 1**, the side chain on BDT units changes from decyl (*n* = 10) to octyl (*n* = 8) and hexyl (*n* = 6), corresponding to the polymer PTAZ-TPD10-C10, PTAZ-TPD10-C8, and PTAZ-TPD10-C6, respectively. As electron acceptors we select three representative materials, i.e., a fullerene acceptor [6,6]-phenyl-C₇₁-butyric acid methyl ester ([70]PCBM),^[16] a polymer acceptor poly{[N,N'-bis(2-octyldodecyl)naphthalene-1,4,5,8-bis(dicarboximide)-2,6-diyl]-*alt*-5,5'-(2,2'-bithiophene)} (N2200),^[17] and a fused-ring small molecular acceptor 3,9-bis(2-methylene-(3-(1,1-dicyanomethylene)indanone)-5,5,11,11-tetrakis(4-hexylphenyl)dithieno[2,3-*d*:2',3'-*d'*]-s-indaceno[1,2-*b*:5,6-*b'*]dithiophene (ITIC)^[18] (**Scheme 1**). Interestingly, distinctly different effects of the side chain length of the polymer donor on the device performance were observed when the polymers were combined with different electron acceptors in PSCs. Upon changing the side chain of PTAZ-TPD10-C_n from decyl to hexyl, the [70]PCBM-based devices show remarkable PCE improvement, whereas the N2200- and ITIC-based devices show monotonically decreased PCEs. Morphology investigation revealed that these different side chain effects originated from the different miscibility between polymer donors and acceptors. Shortening the side chain enables the polymer donor more miscible with [70]PCBM, but makes the polymer donor less miscible with N2200 and ITIC, which in turn leads to contracted domains in [70]PCBM-based blends but enlarged domains in N2200- and ITIC-based blends. These findings provide an important

Table 1. Molecular weights, optical properties, and energy levels of PTAZ-TPD10-C n .

PTAZ-TPD10-C n	M_n [kDa]	\bar{D}_M	λ_{\max} [nm]	λ_{onset} [nm]	E_g^{opt} [eV]	HOMO [eV]	LUMO [eV]	E_g^{CV} [eV]
C10	33	2.5	551, 590	650	1.91	−5.27	−3.24	2.03
C8	36	2.4	551, 577	650	1.91	−5.27	−3.23	2.04
C6	37	2.9	548, 582	650	1.91	−5.26	−3.23	2.03

understanding of structure–property relationships that will guide the development of new donor polymers to match with emerging nonfullerene small molecular acceptors and polymer acceptors.

2. Results and Discussion

2.1. Synthesis of the Polymer Donors

The polymers PTAZ-TPD10-C n are composed of an electron-rich unit BDT, and two electron-deficient units of TAZ and TPD. An important merit of random copolymers is their excellent solubility, which can reduce the complexity for establishing a reliable structure–performance relationship. Moreover, random copolymers are able to afford highly efficient solar cells as well.^[19] The length of the side chains on BDT units varies from decyl ($n = 10$) to octyl ($n = 8$) and hexyl ($n = 6$) (Scheme 1), while the side chains on TAZ units and TPD units are kept to be constant. The copolymers were synthesized by the Stille cross-coupling reaction with reasonable yields. The feeding ratio of BDT:TAZ:TPD for copolymerization is set to 1:0.9:0.1. Benefitting from the random conjugated backbones, all polymers are readily soluble in common solvents such as chloroform (CF), chlorobenzene (CB), and *ortho*-dichlorobenzene (*o*-DCB). Gel permeation chromatography (GPC) measurements performed at 140 °C using *o*-DCB as the eluent suggest that all polymers possess similar number-average molecular weights of $M_n = 35 \pm 2$ kDa and molar-mass dispersity ($\bar{D}_M = M_w/M_n$) of ≈ 2.5 (Table 1). The similar molecular weights are beneficial to a fair comparison of the side chain effects of the polymer donors since molecular weight is an important factor that influence the performance of PSCs.^[7d,20] The thermal stability of PTAZ-TPD10-C n was characterized by thermal gravimetric analysis (TGA) measurements. As shown

in Figure S1 (Supporting Information), all the polymers are very stable with decomposition temperatures corresponding 5% weight loss up to ≈ 450 °C.

2.2. Optical Properties and Energy Levels

The UV–vis absorption spectra of the PTAZ-TPD10-C n polymers in thin films are shown in Figure 1a, and relevant data are listed in Table 1. The absorption spectra in solutions are shown in Figure S2 in the Supporting Information. The PTAZ-TPD10-C n polymers show very similar optical absorption characteristics. The absorption spectra of the polymers in thin films are red-shifted by ≈ 30 nm as compared to those in solutions, suggesting the stronger interchain interactions in solid states. The absorption onset of the PTAZ-TPD10-C n polymers are identical, leading to the same optical bandgap $E_g^{\text{opt}} = 1.91$ eV. The highest occupied molecular orbital (HOMO) and lowest unoccupied molecular orbital (LUMO) energy levels of the polymers were determined by cyclic voltammetry (CV) experiments. The energy levels are depicted in Figure 1b, and the cyclic voltammograms are shown in Figure S3 in the Supporting Information. All PTAZ-TPD10-C n polymers show similar onset potentials for both the oxidation and reduction processes, leading to a very similar HOMO level of ≈ -5.27 eV and a LUMO level of ≈ -3.23 eV. The LUMO–LUMO offsets between PTAZ-TPD10-C n and different electron acceptors ([70]PCBM, N2200, and ITIC) are all larger than 0.3 eV, which is high enough for efficient electron transfer from the excited polymer donors to the excited electron acceptors.^[21] The HOMO–HOMO offsets between PTAZ-TPD10-C n and electron acceptors are estimated to be 0.72 eV for [70]PCBM, 0.50 eV for N2200, and 0.23 eV for ITIC. Although the HOMO–HOMO offsets for ITIC is substantially lower than that for [70]PCBM and N2200, this does not influence the hole transfer

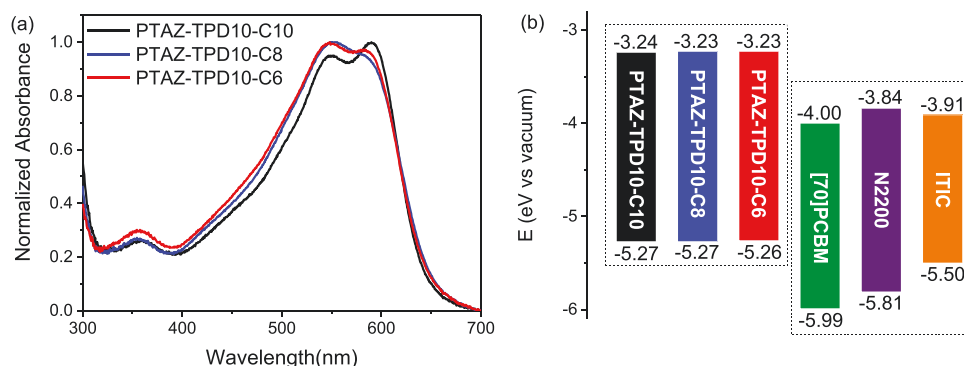


Figure 1. a) Absorption spectra of PTAZ-TPD10-C n in thin films and b) energy levels of PTAZ-TPD10-C n , [70]PCBM, N2200, and ITIC.

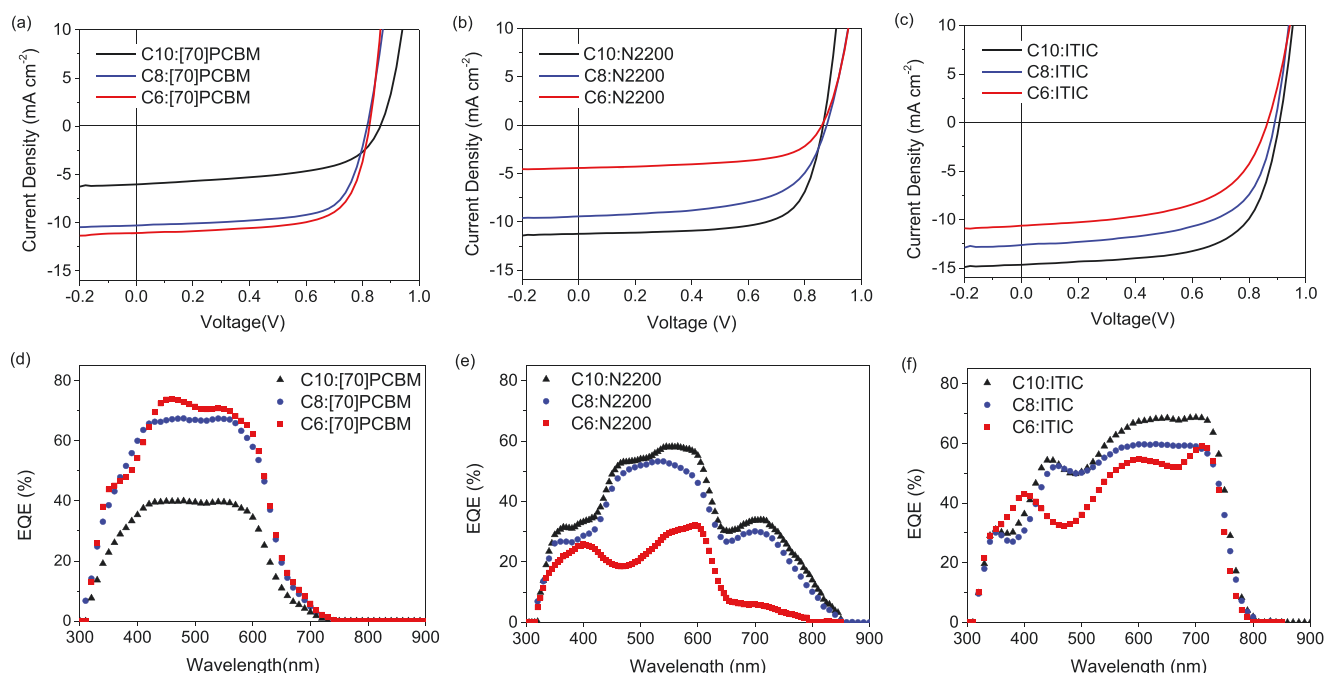


Figure 2. a–c) The J – V curves and b–f) corresponding EQE spectra of the solar cells based on PTAZ-TPD10- C_n :acceptor blends.

from ITIC to the polymer donors PTAZ-TPD10- C_n because hole transfer is very efficient for fused-ring small molecular systems even at very small HOMO–HOMO offsets.^[22] The similar optical absorption characteristics and energy levels of the PTAZ-TPD10- C_n polymers are favorable for investigating the side chain effects on the solar cell performance.

2.3. Solar Cell Characteristics

With the above mentioned three PTAZ-TPD10- C_n polymers, we selected [70]PCBM, N2200, ITIC as the acceptors to form nine donor:acceptor combinations for solar cell fabrication and evaluation. The three acceptors employed in this study are representative fullerene-based, polymer, and small molecular non-fullerene acceptors, respectively. The device configuration of

the solar cells is indium tin oxide (ITO)/poly(3,4-ethylenedioxythiophene):poly(styrenesulfonate) (PEDOT:PSS)/active layer/poly[(9,9-bis(3-(*N,N*-dimethyl)-*N*-ethylammonium)-propyl)-2,7-fluorene]-*alt*-2,7-(9,9-dioctylfluorene)] dibromide (PFN-Br)/Ag. For each polymer:acceptor combination, the device fabrication was fully optimized in terms of polymer:acceptor weight ratio, solvent and type of co-solvent, thermal annealing, and layer thickness. The current density–voltage (J – V) characteristics and external quantum efficiencies (EQEs) of the optimized solar cells are exhibited in **Figure 2**, and the device parameters are summarized in **Table 2**. The J_{sc} was determined by integrating the EQE with the AM1.5G spectrum to accurately estimate the PCEs of the solar cells. The device statistics are summarized in Table S1 in the Supporting Information, and the solar cell performance under various conditions are summarized in Tables S2–S4 in the Supporting Information. **Figure 3** compares

Table 2. Device parameters of the solar cells based on PTAZ-TPD10- C_n :acceptor blends under illumination of AM1.5G (100 mW cm^{−2}).

Acceptor	PTAZ-TPD10- C_n	V_{oc} [V]	J_{sc}^a [mA cm ^{−2}]	FF	PCE [%]
[70]PCBM	C10	0.85	6.0	0.56	2.9
	C8	0.82	10.3	0.64	5.4
	C6	0.82	11.1	0.69	6.3
N2200	C10	0.87	11.2	0.70	6.8
	C8	0.88	9.4	0.60	5.0
	C6	0.86	4.4	0.60	2.3
ITIC	C10	0.91	14.7	0.66	8.8
	C8	0.89	12.6	0.60	6.7
	C6	0.86	10.6	0.60	5.5

^a)Determined by integrating the EQE spectrum with the AM1.5G spectrum.

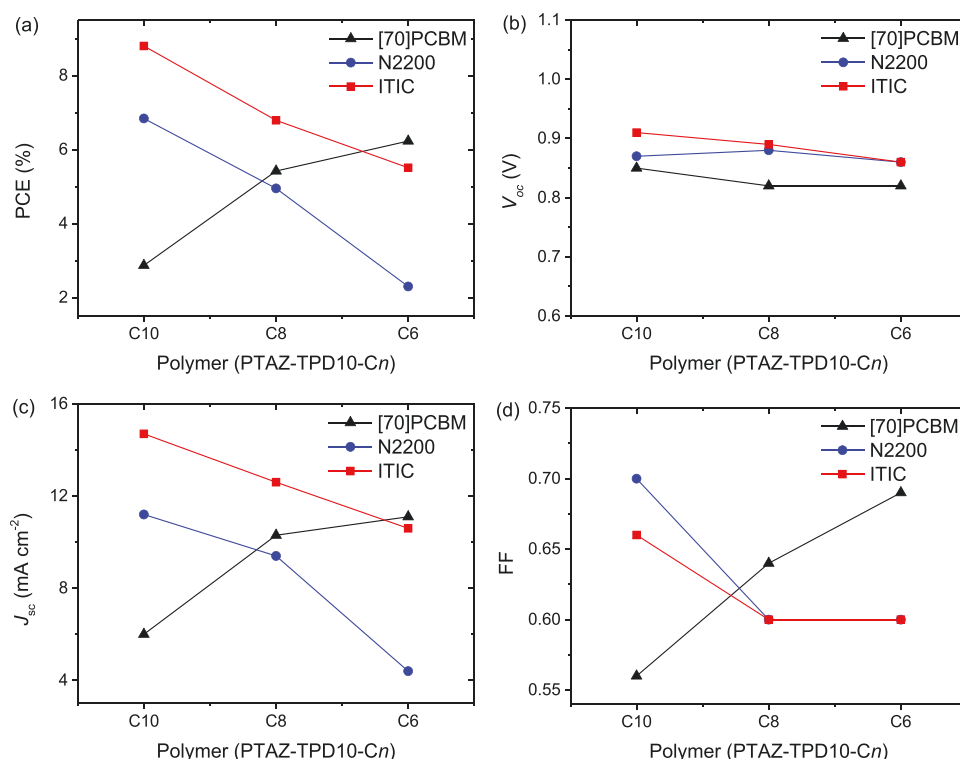


Figure 3. Change of a) PCE, b) V_{oc} , c) J_{sc} , and d) FF with the side chain length of PTAZ-TPD10-*C_n* for the solar cells with various electron acceptors.

the PCE, open-circuit voltage (V_{oc}), short-circuit current density (J_{sc}), and fill factor (FF) of the solar cells with various acceptors as a function of side chain length of PTAZ-TPD10-*C_n*. For [70]PCBM-based devices, the J_{sc} and FF increase monotonically along with shortening the side chain of PTAZ-TPD10-*C_n*. The increase of J_{sc} is verified by EQE spectra (Figure 2b). The EQE maxima increase from 40% for PTAZ-TPD10-C10 to 68% for PTAZ-TPD10-C8 and 74% for PTAZ-TPD10-C6. The V_{oc} of the solar cells is almost unchanged, agreeing well with the similar energy levels of the PTAZ-TPD10-*C_n* polymers. As a result, the PCEs of the PTAZ-TPD10-*C_n*:[70]PCBM solar cells increase from 2.9% to 6.3% upon changing the side chain of PTAZ-TPD10-*C_n* from decyl to hexyl. This side chain effect in fullerene-based devices is consistent with the previous reports based on other polymer donors.^[23] Interestingly, distinctly different characteristics are observed for N2200- and ITIC-based devices. The PCE of the N2200-based devices decreases monotonically from 6.8% to 2.3%, and that of the ITIC-based devices decreases monotonically from 8.8% to 5.5% when shortening the side chain of PTAZ-TPD10-*C_n* from decyl to hexyl. This is mainly caused by the drop of J_{sc} and FF, while the fluctuation of V_{oc} is very small. The EQE spectra of the solar cells further confirm these side chain effects (Figure 2e,f). The EQE drops gradually upon shortening the side chain of PTAZ-TPD10-*C_n* for both N2200- and ITIC-based devices. Such distinctly different side chain effects of polymer donors on solar cells with different electron acceptors suggest that the polymer design rationales established on fullerene-based system is not necessarily applicable to all-polymer solar cells and small molecular nonfullerene solar cells.

2.4. Charge Generation, Transport, and Recombination

Steady-state photoluminescence (PL) quenching experiments were performed to investigate the charge generation characteristics of the blend films. The PL spectra of the pure PTAZ-TPD10-*C_n* polymers and various blend films are shown in Figure S4 in the Supporting Information. The pure PTAZ-TPD10-*C_n* polymers show intense light emission peaked at about 680 nm upon photoexcitation at 580 nm. When blended with the acceptors to form polymer:acceptor bulk-heterojunction films, the PL of the pure PTAZ-TPD10-*C_n* polymers were significantly quenched, suggesting efficient exciton dissociation at the donor:acceptor interface. The PL quenching efficiency (ΔPL) was estimated by the PL intensity of the PTAZ-TPD10-*C_n*:acceptor blends with respect to that of pure PTAZ-TPD10-*C_n* polymers, which were used to evaluate the side chain effect of polymer donors on exciton dissociation. The data is gathered in Table S5 in the Supporting Information. For [70]PCBM-based blend films, the ΔPL increased slightly from 99.23% to 99.82% upon shortening the side chain of the polymer donors, suggesting the improvement of charge generation efficiency. On the contrary, the ΔPL decreased when the PTAZ-TPD10-*C_n* polymers blended with N2200 (from 99.26% to 97.70%) and ITIC (from 99.57% to 99.08%), indicating the drop of charge generation efficiency upon shortening the side chain of polymer donors. Overall, the changes of PL quenching efficiency for various blends upon side chain shortening of PTAZ-TPD10-*C_n* follow the same trends for J_{sc} and EQEs in corresponding solar cells (Figure 3).

The hole and electron mobilities of the PTAZ-TPD10-*C_n*:acceptor blends were measured by space-charge-limited

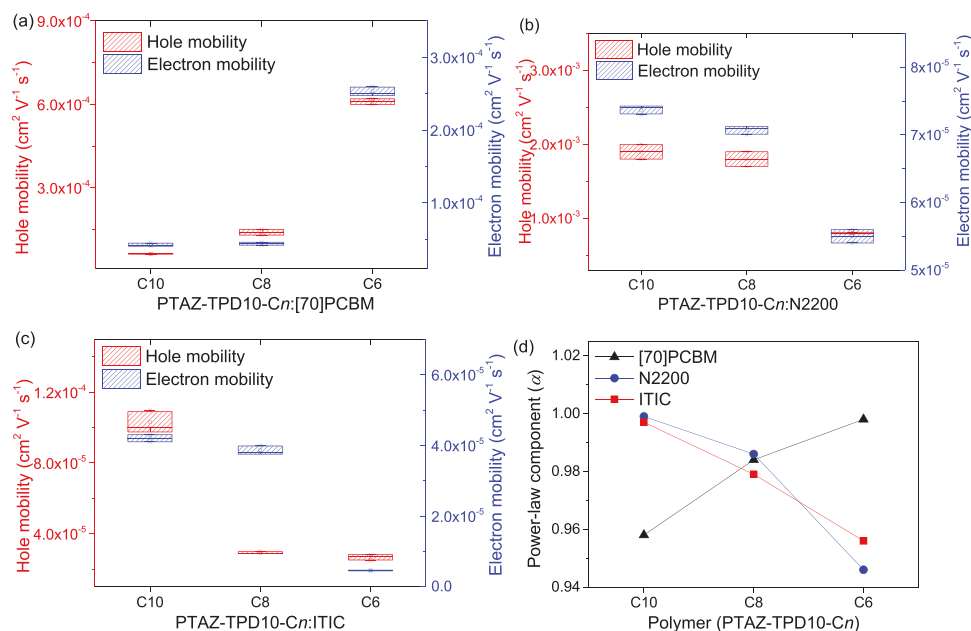


Figure 4. a–c) Hole and electron mobilities of blend films of a) PTAA-TPD10-Cn:[70]PCBM, b) PTAA-TPD10-Cn:N2200, and c) PTAA-TPD10-Cn:ITIC; d) the power-law component (α) of the solar cells of PTAA-TPD10-Cn for various acceptors.

current (SCLC) method in single carrier devices to study the influence of side chain length of polymer donors on charge transport properties in different systems. The results are presented in Table S5 (Supporting information) and Figure 4a–c. Upon shortening the side chain of PTAA-TPD10-Cn, the hole and electron mobilities of the [70]PCBM-based blends show an increasing trend, while those of N2200- and ITIC-based blends drop gradually. The dependence of J_{sc} on intensity of incident light (P_{light}) was measured to investigate the bimolecular charge recombination in devices. The corresponding J_{sc} – P_{light} characteristics in the light intensity range from 1 to 100 mW cm^{-2} are shown in Figure S6 in the Supporting Information. In principle, the J_{sc} shows a power-law dependence on the P_{light} ($J_{sc} \propto P_{light}^\alpha$), where the power-law component (α) will be unity in the case of the absence of bimolecular recombination loss.^[24] In Figure 4d, we plot the α value of the solar cells of PTAA-TPD10-Cn for various acceptors. The α value increases monotonically for the [70]PCBM-based devices, but decreases for N2200- and ITIC-based devices along with shortening the side chain length of PTAA-TPD10-Cn. The J_{sc} and FF of bulk-heterojunction PSCs are greatly affected by the charge transport and recombination characteristics.^[25] The results demonstrated above thus explained the different influence of side chain length of polymer donors on J_{sc} and FF for different electron acceptors.

2.5. Polymer Crystallinity and Bulk-Heterojunction Morphology

The crystalline order of the polymers in both pure films and in PTAA-TPD10-Cn:acceptor blends were characterized by grazing incidence wide-angle X-ray scattering (GIWAXS). The results for the pure polymers are shown in Figure S9 in the Supporting Information, and the results for the blend films

are shown in Figure 5. PCBM showed a totally amorphous structure, while N2200, ITIC, and all three donor polymers have semicrystalline characteristics with mostly face-on morphology, evidenced by clear lamellar and π – π stacking peaks in the in-plane and out-of-plane direction, respectively. In the blend systems, the crystalline behavior of each component retained the same and their characteristic diffraction peaks can be seen in the 1D profile integrated from both in-plane and out-of-plane directions. Table 3 summarized the key parameters for the packing behavior of donor polymer, where both side chain packing and π – π stacking distance were deconvoluted from the combined peak of two components. This is performed through fitting the peak into two independent peaks using Gaussian function, and later comparing with the peak positions of pristine polymer scattering data to determine its origin. For PTAA-TPD10-Cn:[70]PCBM devices, the (010) π – π stacking peak is too weak for a good data fitting. In N2200 and ITIC systems, the π – π stacking distance was barely influenced and no clear trend can be observed. On the other hand, the (100) lamellar packing distance showed obvious decrease with decreasing side chain length, which is similar to pure donor polymers.

The morphology of the PTAA-TPD10-Cn:acceptor blends was further investigated by transmission electron microscopy (TEM) and atomic force microscopy (AFM). The bright-field TEM images are shown in Figure 6. The morphologies of the blend films for each electron acceptor are consistent with the device performance. For the [70]PCBM-based blends, PTAA-TPD10-C10 leads to a clear phase separation with large domain sizes, which are caused by liquid-liquid phase separation during film-deposition due to the too good solubility of PTAA-TPD10-C10. Upon shortening the side chain of the polymer donors, the domains of the blend films contracts significantly. Particularly, the PTAA-TPD10-C6:[70]PCBM blend shows finely dispersed

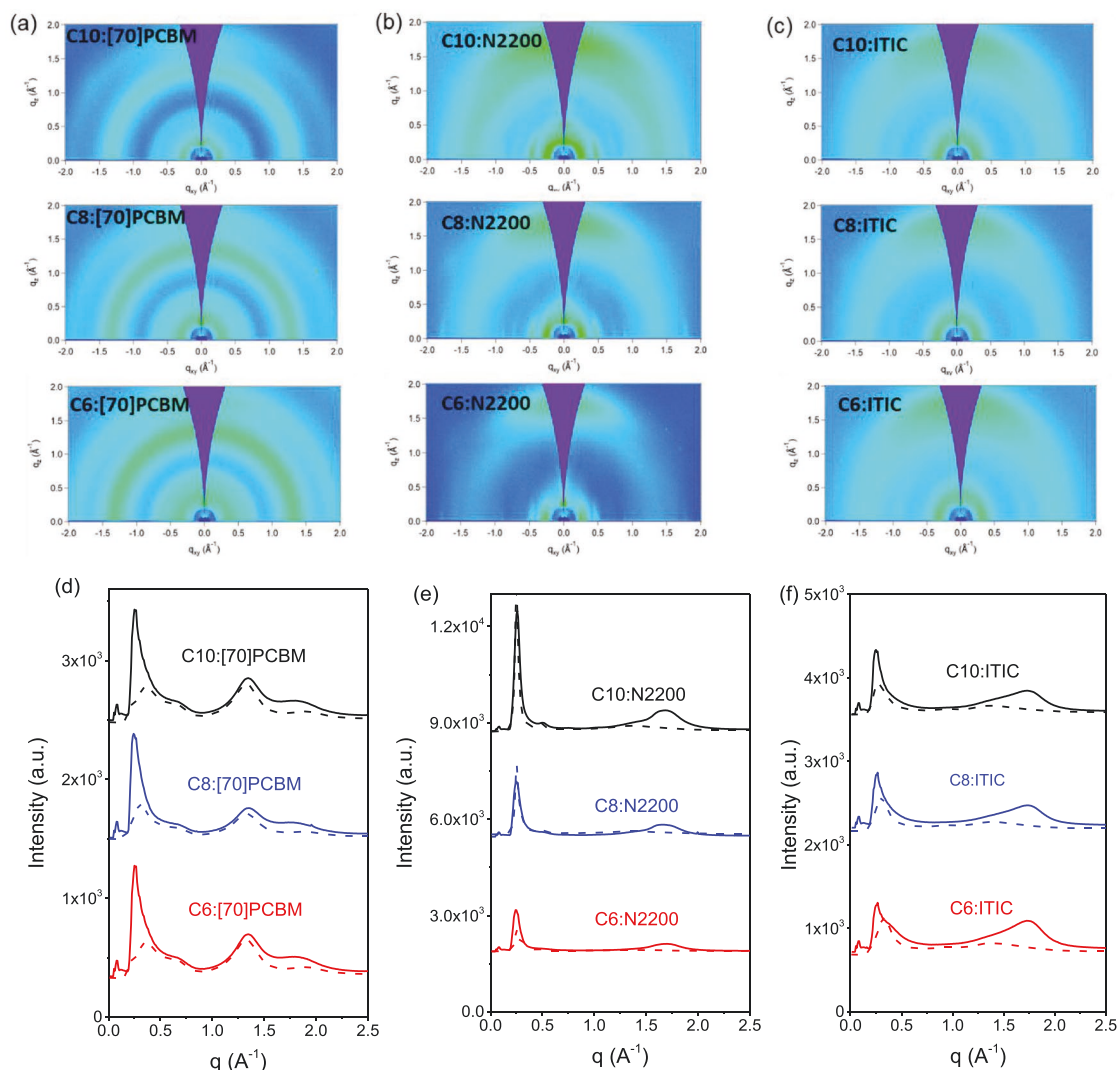


Figure 5. a–c) GIWAXS patterns of PTAZ-TPD10-*C_n*:acceptor blend films: a) PTAZ-TPD10-*C_n*:*[70]*PCBM, b) PTAZ-TPD10-*C_n*:N2200, and c) PTAZ-TPD10-*C_n*:ITIC. d–f) GIWAXS line-cut profiles (solid line: out-of-plane line-cut profile; dotted line: in-plane line-cut profiles) of PTAZ-TPD10-*C_n*:acceptor blend films: d) PTAZ-TPD10-*C_n*:*[70]*PCBM, e) PTAZ-TPD10-*C_n*:N2200, and f) PTAZ-TPD10-*C_n*:ITIC.

structures and fibrillar interpenetrating networks. The morphology evolution in *[70]*PCBM-based blends upon changing the side chains of PTAZ-TPD10-*C_n* is similar to the phenomena observed for other polymer:fullerene systems, for which the liquid-liquid phase separation is suppressed upon reducing the polymer solubility.^[26] However, the N2200- and ITIC-based blends show completely opposite trend of morphology evolution when shortening the side chain of PTAZ-TPD10-*C_n*. The blend films of PTAZ-TPD10-C10:N2200 and PTAZ-TPD10-C10:ITIC are intimately mixed without noteworthy phase separation. Upon shortening the side chain of polymer donors, the blend films of PTAZ-TPD10-*C_n*:N2200 acceptor become less mixed and the contrast between the bright regions and dark regions are more significant, suggesting the N2200-based all-polymer blends are more phase separated for polymer donors with shorter side chains. For ITIC-based blends, it is difficult to differentiate the films made from PTAZ-TPD10-C10 and PTAZ-TPD10-C8 in TEM images, but the film of PTAZ-TPD-C6

shows fibrillar structures with notably larger width, which confirms the formation of more phase separated BHJ morphology.

The AFM height images (Figure S7 in the Supporting Information) and phase images (Figure S8 in the Supporting Information) further verify the morphological changes of the blend films. The *[70]*PCBM-based films exhibit root-mean-square (RMS) roughness of 10.80, 2.90, and 1.15 nm for PTAZ-TPD10-C10, PTAZ-TPD10-C8, and PTAZ-TPD10-C6, respectively. These observations are consistent with the results obtained from TEM, suggesting the mitigation of coarse phase separation in PTAZ-TPD10-*C_n*:*[70]*PCBM by shortening polymer side chain. On the contrary, the RMS roughness of the N2200-based films increases from 1.26 to 1.34 and 2.07 nm going from PTAZ-TPD10-C10 to PTAZ-TPD10-C6. The similar enlargement of RMS roughness is also found for the ITIC-based films, for which the RMS roughness increases from 0.82 to 1.21 and 1.39 nm. The AFM phase images are consistent with the TEM images. Particularly, very clear changes of phase separation for

Table 3. Characteristic length scale of packing phenomenon for donor polymer in blend films of PTAZ-TPD10-C_n:acceptors.

Blend	Lamellar			π -Stacking		
	(100) distance [Å]	FWHM ^{a)} [Å ⁻¹]	CCL ^{b)} [Å]	π - π distance [Å]	FWHM ^{a)} [Å ⁻¹]	CCL ^{b)} [Å]
C10:[70]PCBM	23.53	0.107	58.69	N/A	N/A	N/A
C8:[70]PCBM	20.87	0.154	40.78	N/A	N/A	N/A
C6:[70]PCBM	17.74	0.175	35.89	N/A	N/A	N/A
C10:N2200	25.03	0.036	174.44	3.71	0.275	22.84
C8:N2200	23.35	0.029	216.55	3.73	0.330	19.03
C6:N2200	21.37	0.117	53.68	3.70	0.266	23.61
C10:ITIC	23.79	0.070	89.71	4.08	0.610	10.30
C8:ITIC	21.15	0.099	63.43	4.11	0.570	11.02
C6:ITIC	18.92	0.107	58.69	4.10	0.706	8.90

^{a)}FWHM represents full-width at half maximum; ^{b)}CCL represents crystal coherence length.

PTAZ-TPD10-C_n:ITIC films can be observed from Figure S8g–i (Supporting Information), although these changes are not obvious in TEM images. These results verified the morphological information obtained from TEM images, which reflect the tendency of phase separation in the N2200- and ITIC-based blend films with shortening the side chains of PTAZ-TPD10-C_n.

Time-of-flight secondary ion mass spectroscopy (TOF-SIMS) depth profiling was carried out for elemental analysis in the film. Figure 7 displays the counts of ¹⁹F in the

PTAZ-TPD10-C_n:acceptor blend films versus the sputtering time. In the blend films, we can probe relative vertical phase distribution using the ¹⁹F intensity as fluorine is characteristic for the amount of polymer donor PTAZ-TPD10-C_n. The results suggest clearly different vertical phase distribution profiles for the various PTAZ-TPD10-C_n:acceptor blends. For example, at the beginning stage of sputtering, the ¹⁹F intensity of PTAZ-TPD10-C6:[70]PCBM are less than that of PTAZ-TPD10-C10:[70]PCBM and PTAZ-TPD10-C8:[70]PCBM, indicating that

PTAZ-TPD10-C6 is less enriched at the active layer surface compared to PTAZ-TPD10-C8/C10. At the last stage of sputtering, the ¹⁹F intensity of PTAZ-TPD10-C6:[70]PCBM are higher than that of PTAZ-TPD10-C10:[70]PCBM and PTAZ-TPD10-C8:[70]PCBM, suggesting that PTAZ-TPD10-C6 is more prone to be enriched at the bottom of the active layer than PTAZ-TPD10-C8/10. In this case, the PTAZ-TPD10-C6:[70]PCBM blend shows more favorable vertical phase distribution with the device structure of ITO/PEDOT:PSS/active layer/PFN-Br/Ag, in which the donor is closer to anode interface. This feature facilitates charge extraction and reduces charge recombination, and produces a higher FF and J_{sc} . The TOF-SIMS results of PTAZ-TPD10-C_n:N2200 and PTAZ-TPD10-C_n:ITIC suggest different vertical phase distribution with more polymer donor enriched at the active layer surface and less enriched at the bottom of the active layer upon shortening the side chain length. These results are also consistent with the corresponding solar cell performance.

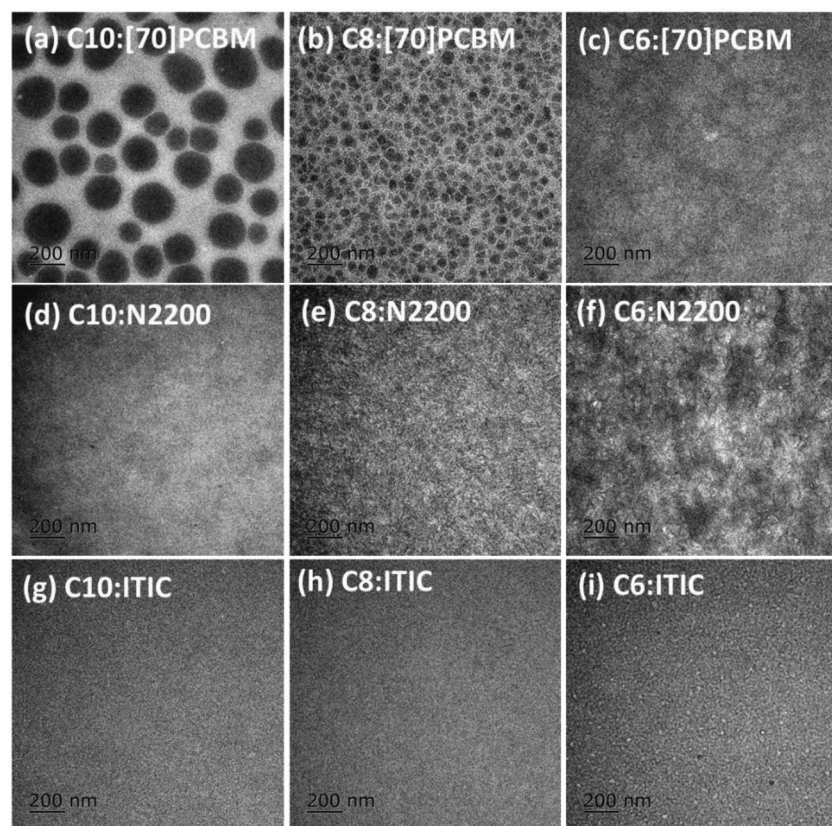


Figure 6. Bright-field TEM images of PTAZ-TPD10-C_n:acceptor blend films: a–c) PTAZ-TPD10-C_n: [70]PCBM, d–f) PTAZ-TPD10-C_n:N2200, g–i) PTAZ-TPD10-C_n:ITIC. The scale bar is 0.2 μ m.

2.6. Solubility and Interaction Parameters

To explain the above correlations, we calculated the solubility parameter (δ) of each material, which can help to analyze the

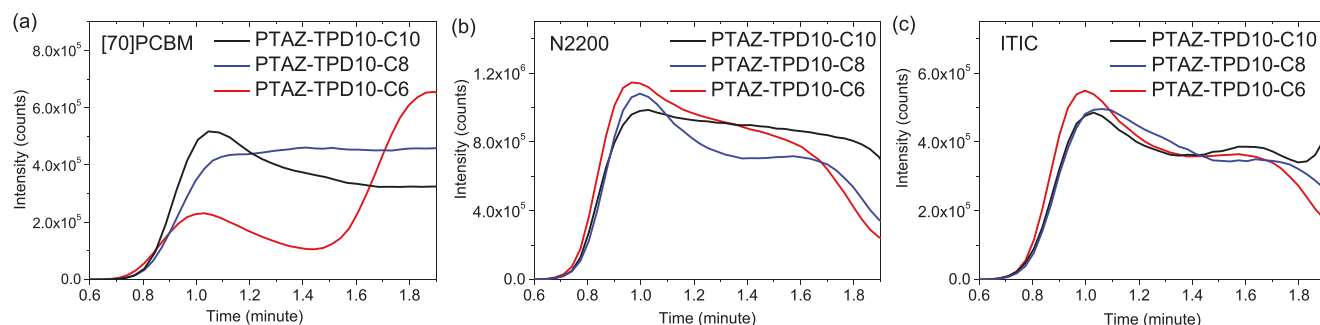


Figure 7. TOF-SIMS depth profiling of the ^{19}F intensity in PTAZ-TPD10-*Cn*:acceptor blend films versus sputtering time: a) PTAZ-TPD10-*Cn*: $^{70}\text{PCBM}$, b) PTAZ-TPD10-*Cn*:N2200, and c) PTAZ-TPD10-*Cn*:ITIC.

miscibility of components in a blend, thus providing understandings for the blend morphology from a point of polymer physics view. If the δ for two components is similar, then they are more miscible in the blend. In other words, if the difference in absolute value ($\Delta\delta$) of two components is smaller, the two components will be more intermixed and less phase separated in blend.^[27] We thus estimated the surface energy of PTAZ-TPD10-*Cn* and N2200 from contact angle measurements, and the surface energies of $^{70}\text{PCBM}$ and ITIC were adopted from literatures.^[28,29] These results are shown in Figure S10 and Table S7 in the Supporting Information. Interestingly, the surface energies of the polymer donors reduce gradually from PTAZ-TPD10-C10 to PTAZ-TPD10-C6, which could be related to the increase of relative content of fluorine in these polymers. We then calculate the solubility parameter from

$$\delta = K\sqrt{\gamma} \quad (1)$$

where γ is the surface energy of the material, K is the proportionality constant ($K = 116 \times 10^3 \text{ m}^{-1/2}$).^[13a,30] The δ values for the materials are summarized in Table S9 in the Supporting Information, and the order of solubility parameter of the materials is depicted in **Figure 8**. The δ values for the polymer donors are in the order of PTAZ-TPD10-C10 > PTAZ-TPD10-C8 > PTAZ-TPD10-C6. Moreover, the δ values of PTAZ-TPD10-*Cn* polymers are all larger than that of $^{70}\text{PCBM}$ but smaller than those of N2200 and ITIC. Thus, the $\Delta\delta$ values for the PTAZ-TPD10-*Cn*: $^{70}\text{PCBM}$ blends follow the order of PTAZ-TPD10-C10 > PTAZ-TPD10-C8 > PTAZ-TPD10-C6. As a result, the shorter side chains of the polymer donors result in a higher tendency of intermixing but lower domain purity in PTAZ-TPD10-*Cn*: $^{70}\text{PCBM}$ blends. Conversely, the $\Delta\delta$ values follow the order of PTAZ-TPD10-C10 < PTAZ-TPD10-C8 < PTAZ-TPD10-C6 for the N2200- and ITIC-based blends, suggesting that the miscibility between the donor and acceptor decrease along with shortening the side chains of PTAZ-TPD10-*Cn*. Consequently, the shorter side chains lead to more pronounced phase separation and larger domain size in N2200- and ITIC-based blends.

The miscibility between two components in a blend can be further discussed using Flory–Huggins interaction parameter χ_{ij} , which can be described as^[31]

$$\chi_{ij} = \frac{V_0}{RT}(\delta_i - \delta_j)^2 \quad (2)$$

where χ_{ij} is the Flory–Huggins interaction parameter between the substance i and j (in this case, the polymer donors PTAZ-TPD10-*Cn* and various electron acceptor materials), V_0 is the geometric mean of the polymer segment molar volume, R is the gas constant, T is the absolute temperature, and δ_i and δ_j are the solubility parameter of substance i and j , respectively. The value χ_{ij} reflects the binary miscibility, and the smaller χ_{ij} value means better miscibility. The results are shown in **Table 4**. The Flory–Huggins interaction parameters for the $^{70}\text{PCBM}$ -based blends are decreasing along with shortening the side chain of PTAZ-TPD10-*Cn*, indicating improved miscibility between the polymer donor and $^{70}\text{PCBM}$, which will result in more intermixed morphology. However, the N2200- and ITIC-based blends show converse trends in Flory–Huggins interaction parameters upon shortening the side chain of PTAZ-TPD10-*Cn*, which will lead to a higher tendency of phase separation in blends.

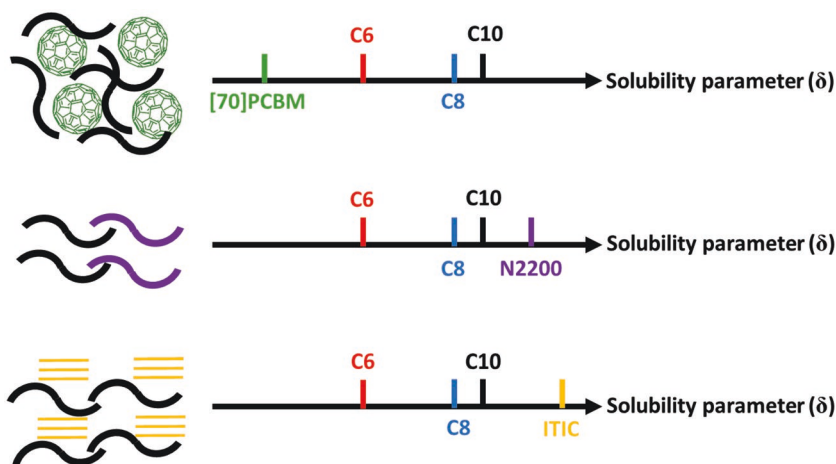


Figure 8. Schematic illustration of the order of solubility parameter of PTAZ-TPD10-*Cn*, $^{70}\text{PCBM}$, N2200, and ITIC.

Table 4. Flory–Huggins interaction parameters for various PTAZ-TPD10-*C_n*:acceptor combinations.

Sample ^{a)}	[70]PCBM	N2200	ITIC
PTAZ-TPD10-C10	$\chi_{14} = 4.28\kappa$	$\chi_{24} = 0.014\kappa$	$\chi_{34} = 1.64\kappa$
PTAZ-TPD10-C8	$\chi_{15} = 2.66\kappa$	$\chi_{25} = 0.31\kappa$	$\chi_{35} = 2.96\kappa$
PTAZ-TPD10-C6	$\chi_{16} = 2.56\kappa$	$\chi_{26} = 0.35\kappa$	$\chi_{36} = 3.06\kappa$

^{a)}Subscripts: 1 = [70]PCBM, 2 = N2200, 3 = ITIC, 4 = PTAZ-TPD10-C10, 5 = PTAZ-TPD10-C8, 6 = PTAZ-TPD10-C6; κ stands for $\frac{V_0}{RT}$.

In this context, the solubility parameter and Flory–Huggins model give reasonable explanations to the morphological characteristics of the blend films of PTAZ-TPD10-*C_n* with various acceptors. However, it is worth pointing out that the BHJ morphology is kinetically frozen in during spin coating due to the rapid evaporation of solvent. This nonequilibrium morphology can be affected by many factors such as solvent, additive, annealing temperature, spin speed, etc. Enabling the morphology to evolve to a thermodynamic equilibrium state is needed to elucidate the side chain effect of PTAZ-TPD10-*C_n* polymers on the phase behavior of the resulting BHJ blends by means of solubility parameter and Flory–Huggins model. Possible methods include annealing the deposited blend film above the glass transition temperature of one or both components or exposing the sample to a solvent vapor. Moreover, the PTAZ-TPD10-*C_n* polymers are all semicrystalline as shown in Figure S9 and Table S6 in the Supporting Information, which contain both amorphous and crystalline regions. When the polymers are blended with different acceptors, the crystallization processes of BHJ components would complicate phase separation further.

Based on the characterizations of optoelectronic properties and morphology demonstrated above, the relationships between the side chain length of PTAZ-TPD10-*C_n* and the device performance of solar cells for different electron acceptors can be reasonably correlated. Upon shortening the side chains of PTAZ-TPD10-*C_n*, the PTAZ-TPD10-*C_n*: [70]PCBM blends tend to form more proper phase separation morphology with smaller domain size, bicontinuous interpenetrating networks, and more favorable vertical phase distribution, which in turn lead to more efficient charge generation via increased donor:acceptor interface area, improved charge transport and suppressed charge recombination. For the N2200- and ITIC-based blends, shortening the side chain of PTAZ-TPD10-*C_n* results in opposite effects on the blend morphology and vertical phase distribution, which deteriorates charge generation and transport but facilitates charge recombination.

3. Conclusion

In conclusion, a set of random copolymers PTAZ-TPD10-*C_n* possessing the same conjugated backbones but different length of alkyl side chains were synthesized to investigate the effect of the length of side chain of the polymer donors on the device performance of solar cells with different electron acceptors ([70]PCBM, N2200, and ITIC in this study). Interestingly, the J_{sc} , FF, and PCE of the [70]PCBM-based solar cells

decrease with shortening the side chains of PTAZ-TPD10-*C_n*, while the N2200- and ITIC-based solar cells show opposite trends. Detailed morphology studies show that shortening the side chains of PTAZ-TPD10-*C_n* lead to more intermixed morphology, contracted domains, and favorable vertical phase distribution in [70]PCBM-based blends but converse effects in N2200- and ITIC-based blends. As a result, shortening the side chains of PTAZ-TPD10-*C_n* facilitates charge generation and transport and suppresses bimolecular recombination for [70]PCBM-based devices, but exerts converse influence on the N2200- and ITIC-based devices. The solubility parameter and Flory–Huggins interaction parameter determination for the materials from contact angle measurements explain well with the phase separation behavior. More importantly, our study suggests that the experiences of polymer design established on fullerene-based solar cells are not necessarily applicable to nonfullerene solar cells. Moreover, a very recent work of Ade and coworkers^[32] has reported a somewhat opposite result which demonstrated that the donor polymers with shorter alkyl chains work better with a small molecular nonfullerene acceptor. These results further confirmed that not all donor polymers show the same side chain dependence with nonfullerene acceptors. We hope these findings will guide the development of new donor polymers to match with emerging nonfullerene small molecular acceptors and polymer acceptors.

Supporting Information

Supporting Information is available from the Wiley Online Library or from the author.

Acknowledgements

The research was financially supported by the Ministry of Science and Technology (Grant Nos. 2017YFA0206600 and 2014CB643501), and the Natural Science Foundation of China (Grant Nos. 21875072 and 21520102006). S.Z. and X.G. thank financial support from National Science Foundation of U.S. (EPSCOR 8006123 RFA1). Use of the Stanford Synchrotron Radiation Lightsource, SLAC National Accelerator Laboratory, was supported by the U.S. Department of Energy, Office of Science, Office of Basic Energy Sciences under Contract No. DE-AC02-76SF00515. This research used resources of the Advanced Light Source, which is a DOE Office of Science User Facility under contract no. DE-AC02-05CH11231.

Conflict of Interest

The authors declare no conflict of interest.

Keywords

device performance, morphology, polymer donors, polymer solar cells, side chains

Received: May 30, 2019
Published online:

- [1] a) J. J. M. Halls, C. A. Walsh, N. C. Greenham, E. A. Marseglia, R. H. Friend, S. C. Moratti, A. B. Holmes, *Nature* **1995**, 376, 498; b) G. Yu, J. Gao, J. C. Hummelen, F. Wudl, A. J. Heeger, *Science* **1995**, 270, 1789; c) L. Lu, T. Zheng, Q. Wu, A. M. Schneider, D. Zhao, L. Yu, *Chem. Rev.* **2015**, 115, 12666.
- [2] a) W. Ma, C. Yang, X. Gong, K. Lee, A. J. Heeger, *Adv. Funct. Mater.* **2005**, 15, 1617; b) E. Wang, L. Wang, L. Lan, C. Luo, W. Zhuang, J. Peng, Y. Cao, *Appl. Phys. Lett.* **2008**, 92, 033307; c) L. Meng, Y. Zhang, X. Wan, C. Li, X. Zhang, Y. Wang, X. Ke, Z. Xiao, L. Ding, R. Xia, H.-L. Yip, Y. Cao, Y. Chen, *Science* **2018**, 361, 1094.
- [3] X. Du, T. Heumueller, W. Gruber, A. Classen, T. Unruh, N. Li, C. J. Brabec, *Joule* **2019**, 3, 215.
- [4] a) C. B. Nielsen, S. Holliday, H.-Y. Chen, S. J. Cryer, I. McCulloch, *Acc. Chem. Res.* **2015**, 48, 2803; b) C. Yan, S. Barlow, Z. Wang, H. Yan, A. K.-Y. Jen, S. R. Marder, X. Zhan, *Nat. Rev. Mater.* **2018**, 3, 18003; c) P. Cheng, G. Li, X. Zhan, Y. Yang, *Nat. Photonics* **2018**, 12, 131; d) J. E. Coughlin, Z. B. Henson, G. C. Welch, G. C. Bazan, *Acc. Chem. Res.* **2014**, 47, 257; e) G. Zhang, J. Zhao, P. C. Y. Chow, K. Jiang, J. Zhang, Z. Zhu, J. Zhang, F. Huang, H. Yan, *Chem. Rev.* **2018**, 118, 3447; f) W. Gao, T. Liu, C. Zhong, G. Zhang, Y. Zhang, R. Ming, L. Zhang, J. Xin, K. Wu, Y. Guo, W. Ma, H. Yan, Y. Liu, C. Yang, *ACS Energy Lett.* **2018**, 3, 1760; g) W. Gao, T. Liu, R. Ming, Z. Luo, K. Wu, L. Zhang, J. Xin, D. Xie, G. Zhang, W. Ma, H. Yan, C. Yang, *Adv. Funct. Mater.* **2018**, 28, 1803128; h) W. Gao, M. Zhang, T. Liu, R. Ming, Q. An, K. Wu, D. Xie, Z. Luo, C. Zhong, F. Liu, F. Zhang, H. Yan, C. Yang, *Adv. Mater.* **2018**, 30, 1800052; i) Z. Luo, H. Bin, T. Liu, Z.-G. Zhang, Y. Yang, C. Zhong, B. Qiu, G. Li, W. Gao, D. Xie, K. Wu, Y. Sun, F. Liu, Y. Li, C. Yang, *Adv. Mater.* **2018**, 30, 1706124.
- [5] a) J. Chen, Y. Cao, *Acc. Chem. Res.* **2009**, 42, 1709; b) C. Duan, F. Huang, Y. Cao, *J. Mater. Chem.* **2012**, 22, 10416; c) Y. Li, *Acc. Chem. Res.* **2012**, 45, 723; d) S. Xiao, Q. Zhang, W. You, *Adv. Mater.* **2017**, 29, 1601391.
- [6] a) R. Qin, W. Li, C. Li, C. Du, C. Veit, H.-F. Schleiermacher, M. Andersson, Z. Bo, Z. Liu, O. Inganäs, U. Wurfel, F. Zhang, *J. Am. Chem. Soc.* **2009**, 131, 14612; b) A. C. Stuart, J. R. Tumbleston, H. Zhou, W. Li, S. Liu, H. Ade, W. You, *J. Am. Chem. Soc.* **2013**, 135, 1806; c) Y. Liu, J. Zhao, Z. Li, C. Mu, W. Ma, H. Hu, K. Jiang, H. Lin, H. Ade, H. Yan, *Nat. Commun.* **2014**, 5, 5293; d) H. Hu, P. C. Y. Chow, G. Zhang, T. Ma, J. Liu, G. Yang, H. Yan, *Acc. Chem. Res.* **2017**, 50, 2519.
- [7] a) W. Li, L. Yang, J. R. Tumbleston, L. Yan, H. Ade, W. You, *Adv. Mater.* **2014**, 26, 4456; b) R. C. Coffin, J. Peet, J. Rogers, G. C. Bazan, *Nat. Chem.* **2009**, 1, 657; c) J. Subbiah, B. Purushothaman, M. Chen, T. Qin, M. Gao, D. Vak, F. H. Scholes, X. Chen, S. E. Watkins, G. J. Wilson, A. B. Holmes, W. W. H. Wong, D. J. Jones, *Adv. Mater.* **2015**, 27, 702; d) W. Xiong, F. Qi, T. Liu, L. Huo, X. Xue, Z. Bi, Y. Zhang, W. Ma, M. Wan, J. Liu, Y. Sun, *Sol. RRL* **2018**, 2, 1800129.
- [8] Z. Li, K. Jiang, G. Yang, J. Y. L. Lai, T. Ma, J. Zhao, W. Ma, H. Yan, *Nat. Commun.* **2016**, 7, 13094.
- [9] a) N. Zhou, A. S. Dudnik, T. I. N. G. Li, E. F. Manley, T. J. Aldrich, P. Guo, H.-C. Liao, Z. Chen, L. X. Chen, R. P. H. Chang, A. Facchetti, M. O. de la Cruz, T. J. Marks, *J. Am. Chem. Soc.* **2016**, 138, 1240; b) G. Wang, N. D. Eastham, T. J. Aldrich, B. Ma, E. F. Manley, Z. Chen, L. X. Chen, M. O. de la Cruz, R. P. H. Chang, F. S. Melkonyan, A. Facchetti, T. J. Marks, *Adv. Energy Mater.* **2018**, 8, 1702173.
- [10] H. Fu, Z. Wang, Y. Sun, *Angew. Chem. Int. Ed.* **2019**, 58, 4442.
- [11] a) D. Liu, B. Yang, B. Jang, B. Xu, S. Zhang, C. He, H. Y. Woo, J. Hou, *Energy Environ. Sci.* **2017**, 10, 546; b) Y. Wu, C. An, L. Shi, L. Yang, Y. Qin, N. Liang, C. He, Z. Wang, J. Hou, *Angew. Chem., Int. Ed.* **2018**, 57, 12911.
- [12] a) W. Li, K. H. Hendriks, A. Furlan, W. S. C. Roelofs, S. C. J. Meskers, M. M. Wienk, R. A. J. Janssen, *Adv. Mater.* **2014**, 26, 1565; b) T. Liu, L. Huo, S. Chandrabose, K. Chen, G. Han, F. Qi, X. Meng, D. Xie, W. Ma, Y. Yi, J. M. Hodgkiss, F. Liu, J. Wang, C. Yang, Y. Sun, *Nat. Commun.* **2015**, 6, 1707353; c) C. Lee, H. Kang, W. Lee, T. Kim, K.-H. Kim, H. Y. Woo, C. Wang, B. J. Kim, *Adv. Mater.* **2015**, 27, 2466; d) C. Duan, R. E. M. Willems, J. J. van Franeker, B. J. Bruijnsaers, M. M. Wienk, R. A. J. Janssen, *J. Mater. Chem. A* **2016**, 4, 1855; e) Z.-G. Zhang, Y. Li, *Sci. China: Chem.* **2015**, 58, 192; f) J. Zhao, Y. Li, G. Yang, K. Jiang, H. Lin, H. Ade, W. Ma, H. Yan, *Nat. Energy* **2016**, 1, 15027; g) T. Kurosawa, X. Gu, K. L. Gu, Y. Zhou, H. Yan, C. Wang, G. J. N. Wang, M. F. Toney, Z. Bao, *Adv. Energy Mater.* **2018**, 8, 1701552; h) W. Lee, C. Lee, H. Yu, D.-J. Kim, C. Wang, H. Y. Woo, J. H. Oh, B. J. Kim, *Adv. Funct. Mater.* **2016**, 26, 1543; i) J. Oh, K. Kranthiraja, C. Lee, K. Gunasekar, S. Kim, B. Ma, B. J. Kim, S.-H. Jin, *Adv. Mater.* **2016**, 28, 10016.
- [13] a) S. Kouijzer, J. J. Michels, M. van den Berg, V. S. Gevaerts, M. Turbiez, M. M. Wienk, R. A. J. Janssen, *J. Am. Chem. Soc.* **2013**, 135, 12057; b) J. J. van Franeker, M. Turbiez, W. Li, M. M. Wienk, R. A. J. Janssen, *Nat. Commun.* **2015**, 6, 6229.
- [14] S. Chen, L. Zhang, C. Ma, D. Meng, J. Zhang, G. Zhang, Z. Li, P. C. Y. Chow, W. Ma, Z. Wang, K. S. Wong, H. Ade, H. Yan, *Adv. Energy Mater.* **2018**, 8, 1702427.
- [15] C. Wang, K. Nakano, H. F. Lee, Y. Chen, Y.-L. Hong, Y. Nishiyama, K. Tajima, *Angew. Chem., Int. Ed.* **2018**, 57, 7034.
- [16] M. M. Wienk, J. M. Kroon, W. J. H. Verhees, J. Knol, J. C. Hummelen, P. A. van Hal, R. A. J. Janssen, *Angew. Chem., Int. Ed.* **2003**, 42, 3371.
- [17] H. Yan, Z. Chen, Y. Zheng, C. Newman, J. R. Quinn, F. Dötz, M. Kastler, A. Facchetti, *Nature* **2009**, 457, 679.
- [18] Y. Lin, J. Wang, Z.-G. Zhang, H. Bai, Y. Li, D. Zhu, X. Zhan, *Adv. Mater.* **2015**, 27, 1170.
- [19] a) C. Duan, K. Gao, J. J. van Franeker, F. Liu, M. M. Wienk, R. A. J. Janssen, *J. Am. Chem. Soc.* **2016**, 138, 10782; b) Z. Li, X. Xu, W. Zhang, X. Meng, W. Ma, A. Yartsev, O. Inganäs, M. R. Andersson, R. A. J. Janssen, E. Wang, *J. Am. Chem. Soc.* **2016**, 138, 10935; c) Y.-J. Hwang, T. Earmme, B. A. E. Courtright, F. N. Eberle, S. A. Jenekhe, *J. Am. Chem. Soc.* **2015**, 137, 4424; d) C. Duan, Z. Li, S. Pang, Y.-L. Zhu, B. Lin, F. J. M. Colberts, P. J. Leenaers, E. Wang, Z.-Y. Sun, W. Ma, S. C. J. Meskers, R. A. J. Janssen, *Sol. RRL* **2018**, 2, 1800247; e) J. Kim, S. Park, S. Lee, H. Ahn, S. Joe, B. J. Kim, H. J. Son, *Adv. Energy Mater.* **2018**, 8, 1801601; f) Y. Cui, H. Yao, L. Hong, T. Zhang, Y. Xu, K. Xian, B. Gao, J. Qin, J. Zhang, Z. Wei, J. Hou, *Adv. Mater.* **2019**, 31, 1808356.
- [20] a) S. Chen, Y. An, G. K. Dutta, Y. Kim, Z.-G. Zhang, Y. Li, C. Yan, *Adv. Funct. Mater.* **2017**, 27, 1603564; b) B. Fan, L. Ying, Z. Wang, B. He, X. Jiang, F. Huang, Y. Cao, *Energy Environ. Sci.* **2017**, 10, 1243; c) K. D. Deshmukh, R. Matsidik, S. K. K. Prasad, L. A. Connal, A. C. Y. Liu, E. Gann, L. Thomsen, J. M. Hodgkiss, M. Sommer, C. R. McNeill, *Adv. Funct. Mater.* **2018**, 28, 1707185.
- [21] M. C. Scharber, D. Mühlbacher, M. Koppe, P. Denk, C. Waldauf, A. J. Heeger, C. J. Brabec, *Adv. Mater.* **2006**, 18, 789.
- [22] a) Z. Zheng, O. M. Awartani, B. Gautam, D. Liu, Y. Qin, W. Li, A. Bataller, K. Gundogdu, H. Ade, J. Hou, *Adv. Mater.* **2017**, 29, 1604241; b) J. Hou, O. Inganäs, R. H. Friend, F. Gao, *Nat. Mater.* **2018**, 17, 119; c) S. Chen, Y. Wang, L. Zhang, J. Zhao, Y. Chen, D. Zhu, H. Yao, G. Zhang, W. Ma, R. H. Friend, P. C. Y. Chow, F. Gao, H. Yan, *Adv. Mater.* **2018**, 30, 1804215; d) S. Li, L. Zhan, C. Sun, H. Zhu, G. Zhou, W. Yang, M. Shi, C.-Z. Li, J. Hou, Y. Li, H. Chen, *J. Am. Chem. Soc.* **2019**, 141, 3073.
- [23] D. Xia, Y. Wu, Q. Wang, A. Zhang, C. Li, Y. Lin, F. J. M. Colberts, J. J. van Franeker, R. A. J. Janssen, X. Zhan, W. Hu, Z. Tang, W. Ma, W. Li, *Macromolecules* **2016**, 49, 6445.
- [24] a) L. J. A. Koster, V. D. Mihailetschi, R. Ramaker, P. W. Blom, *Appl. Phys. Lett.* **2005**, 86, 123509; b) M. Mandoc, F. Kooistra, J. Hummelen, B. De Boer, P. Blom, *Appl. Phys. Lett.* **2007**, 91,

- 263505; c) S. R. Cowan, A. Roy, A. J. Heeger, *Phys. Rev. B* **2010**, *82*, 245207.
- [25] a) C. G. Shuttle, R. Hamilton, B. C. O'Regan, J. Nelson, J. R. Durrant, *Proc. Natl. Acad. Sci. USA* **2010**, *107*, 16448; b) R. A. J. Janssen, J. Nelson, *Adv. Mater.* **2013**, *25*, 1847; c) U. Würfel, D. Neher, A. Spies, S. Albrecht, *Nat. Commun.* **2015**, *6*, 6951; d) I. Ramirez, M. Causá, Y. Zhong, N. Banerji, M. Riede, *Adv. Energy Mater.* **2018**, *8*, 1703551.
- [26] J. J. van Franeker, G. H. L. Heintges, C. Schaefer, G. Portale, W. Li, M. M. Wienk, P. van der Schoot, R. A. J. Janssen, *J. Am. Chem. Soc.* **2015**, *137*, 11783.
- [27] a) L. Ye, H. Hu, M. Ghasemi, T. H. Wang, B. A. Collins, J. H. Kim, K. Jiang, J. H. Carpenter, H. Li, Z. Li, T. McAfee, J. Zhao, X. Chen, J. L. Y. Lai, T. Ma, J.-L. Brédas, H. Yan, H. Ade, *Nat. Mater.* **2018**, *17*, 253; b) L. Ye, B. A. Collins, X. C. Jiao, J. B. Zhao, H. Yan, H. Ade, *Adv. Energy Mater.* **2018**, *8*, 1703058; c) X. Liu, C. Zhang, C. Duan, M. Li, Z. Hu, J. Wang, F. Liu, N. Li, C. J. Brabec, R. A. J. Janssen, G. C. Bazan, F. Huang, Y. Cao, *J. Am. Chem. Soc.* **2018**, *140*, 8934; d) K.-H. Kim, H. Kang, H. J. Kim, P. S. Kim, S. C. Yoon, B. J. Kim, *Chem. Mater.* **2012**, *24*, 2373.
- [28] J. J. van Franeker, D. Hermida-Merino, C. Gommès, K. Arapov, J. J. Michels, R. A. J. Janssen, G. Portale, *Adv. Funct. Mater.* **2017**, *27*, 1702516.
- [29] X. Liu, B. Xie, C. Duan, Z. Wang, B. Fan, K. Zhang, B. Lin, F. J. M. Colberts, W. Ma, R. A. J. Janssen, F. Huang, Y. Cao, *J. Mater. Chem. A* **2018**, *6*, 395.
- [30] S. Nilsson, A. Bernasik, A. Budkowski, E. Moons, *Macromolecules* **2007**, *40*, 8291.
- [31] P. J. Flory, *Principles of Polymer Chemistry*, Cornell University Press, Ithaca, NY **1953**.
- [32] L. Ye, W. Li, X. Guo, M. Zhang, H. Ade, *Chem. Mater.* **2019**, <https://doi.org/10.1021/acs.chemmater.9b00174>.